Correlation between Deposition Parameters and Hydrogen Production in CuO Nanostructured Thin Films

Gianluca A. Artioli[1], Alessandro Mancini[1], Victoria Raissa Barbieri[1], Matteo C. Quattrini[1], Eliana Quartarone[1], Maria Cristina Mozzati[2], Giovanni Drera[3], Luigi Sangaletti[3], Valentina Gombac[4], Paolo Fornasiero[4], Lorenzo Malavasi[1,*]

[1]*Department of Chemistry and INSTM, University of Pavia, Pavia 27100, IT*

[2]*Department of Physics and CNISM, University of Pavia, Pavia 27100, IT*

[3]*I-LAMP and Dipartimento di Matematica e Fisica, Università Cattolica del Sacro Cuore, 25121 Brescia, IT*

[4]*Department of Chemical and Pharmaceutical Sciences ICCOM-CNR Trieste Research Unit, and INSTM Research Unit Trieste University, Trieste 34127, IT*

ABSTRACT

In this paper is reported a systematic investigation of the role of: i) substrate temperature, ii) oxygen partial pressure, and iii) RF-power on the crystal structure and morphology of CuO nanostructured thin films prepared by means of RF-magnetron sputtering starting from a Cu metal target. On selected films have been carried out photocatalytic test in order to correlate the structural and morphological properties of the thin films prepared under different conditions, with the photocatalytic properties to find out the key parameters to optimize the CuO nanostructured films. All the synthesized films are single phase and made of nanorods of variable diameter between 80 and 200 nm. Better aligned rods were obtained at relatively low substrate temperatures and from low to intermediate oxygen partial pressures, resulting in more efficient catalytic activities. Our investigation suggests a relevant role of the crystallographic orientation of the CuO tenorite film on the catalytic activity, as demonstrated by the significant improvement in the H_2 evolution for highly oriented films.

Corresponding Author: Prof. Lorenzo Malavasi; email: lorenzo.malavasi@unipv.it; tel.: +39-382 987921; fax; + 39 382 987575.

INTRODUCTION

The serious concerns related to the future shortage of fossil fuels together with the need of reducing the correlated pollution emissions, including the "greenhouse gas" CO_2, are promoting an active research towards alternative "clean" energy sources and vectors. Among various options [1], the so called "hydrogen economy" represents one of the most appealing opportunity, with the main advantage related to the possibility of converting hydrogen into electricity with high efficiency in a fuel cell without the production of CO_2. In this context, the photocatalytic production of hydrogen by means of solar light driven water splitting is an extremely promising and environmentally friendly route for the hydrogen production [2, 3].

As in other fields of "clean energy" the research on photocatalytic hydrogen production strongly focused on the discovery and optimization of materials capable of driving the required processes under visible light. Starting from the discovery of photoinduced hydrogen production from TiO_2 [4], several other semiconductors have been considered based on their bandgap characteristics and, in particular, on the positions of the valence and conduction band edges relative to the redox potentials of water [5]. Among these, WO_3 [6, 7], Fe_2O_3 polymorphs [8-10], CuO and Cu_2O [11-14], and various titanates [15], nitrides [16], carbides [17, 18] have been extensively explored.

While water splitting has been proved to occur on many inorganic materials, its technological application is still far to be a reality as some limitations must be still overcome, such as the significant reduction of the undesirable hole/electron recombination, the increase of light absorption, especially of the most abundant visible part of the spectrum, and the suppression of the thermodynamically favored backward reaction of H_2 with O_2 to form H_2O [3]. Since water oxidation to O_2 is the most challenging part of water splitting, the hydrogen evolution reaction (HER) is strongly enhanced when a sacrificial organic substrate is used. In this case, the easier oxidation of the sacrificial agent with respect to water has also the advantage to avoid the concomitant formation of H_2 and O_2 that can

recombine. In this contest, particularly appealing sacrificial agents are second generation biomass derivate oxygenate molecules, such as bio-methanol, bio-ethanol or glycerol, the oxidation of which can be also partial and selective to added value by-products. [19-21].

Copper oxides show appealing properties that can be profitably used in the application of such materials as photocathode in photoelectrochemical (PEC) cells. Cu_2O is a p-type direct bandgap (bg) material with a bg of 2.0-2.6 eV. The conduction band (CB) lies at a higher energy (more negative reduction potential) than the potential of the proton reduction half reaction, indicating the suitability of this material for HER. The predicted conversion efficiency of Cu_2O is around 20% [22, 23] which makes it a very promising material, however, the poor stability in aqueous solutions under illumination strongly limits its applicability. On the other hand, CuO is an indirect bandgap material with bg varying from 1.3 to 2.1 eV [24-27]. Despite this ideal bg range for solar light absorption, the efficiency of CuO in solar cells is relatively low. This is in part due to the fact that the CB lies very close in energy than the potential of the proton reduction half reaction, indicating the key importance of nanostructure to drive the correct CB position to allow HER.

To overcome some of these limitations, in many cases the copper oxides have been used in combination with other metal oxides, such as TiO_2. The interaction with titanium oxide by heterojunction may enhance protection against photo-degradation [5, 28]. In addition, the coupling of these two semiconductors improves the separation of the photogenerated carriers, due to a very efficient interparticle charge-transfer process [29-31]. Moreover, a correlation between the carrier recombination and the size of the copper oxides crystallites has been observed [32]. Another recent approach proposed the preparation of Cu_2O/CuO composites made of a thin layer of Cu_2O with a thin film of CuO on its top as a protecting coating, which showed good PEC activity in particular for preferentially oriented Cu_2O layers [33]. CuO as a photocathode in PEC processes has been also prepared in different nanostructured forms such as nanowires, nanorods, etc., in order to correlate the

structure at the nanoscale with the electrochemical properties [for a recent review see Ref. 34 and references therein].

The possible large scale use of CuO as a photocathode in PEC processes requires the preparation of supported (nano)materials with cost-effective and scalable processes. In this regard, the deposition of nanocrystalline CuO thin films represents the most effective process in order to obtain useful materials for applications. Thin films of CuO have been deposited by means of several techniques such as Chemical Vapor Deposition (CVD) [35], spray-pyrolysis [36], electro deposition [37-40], and sputtering [41]. Among these, sputtering is certainly the most suited for low-cost and large-scale production of CuO nanostructured thin films; in addition, sputtering has the advantageous features of controlling the chemical composition and film thickness, high deposition rates, and low substrate heating during deposition.

In the current literature there are several reports regarding the growth of CuO thin films by means of sputtering in both radio-frequency (RF) [42] and direct-current (DC) [43] set-up. Usually, a copper metal target is used and the thin films growth is carried out under a reactive atmosphere containing oxygen. There has been some efforts directed towards the study of the correlation between the sputtering deposition parameters and the crystal structure/nanostructure of the grown films, such as the influence of oxygen pressure [44-47], substrate temperature [48] and RF-power [49]. It should be noted, however, that in all the available references just one deposition parameter at time has been considered and that a comprehensive correlation between the different sputtering depositions parameters and the final structures/nanostructures observed is not straightforward due to the several different sputtering apparatus and set-up used. Finally, notwithstanding the importance of CuO as photoactive materials, very few papers correlated the observed variations resulting from the deposition parameters tuning with the photocatalytic activity.

In view of these considerations, in this paper we carried out a systematic investigation of the role of: i) substrate temperature, ii) oxygen partial pressure, and iii) RF-power on the crystal structure

and morphology of CuO nanostructured thin films. In addition, on selected films for each series, we performed photocatalytic test in order to correlate the structural and morphological properties of the thin films prepared under different conditions, with the photocatalytic properties to find out the key parameters to optimize the CuO nanostructured films.

EXPERIMENTAL

Thin films of copper oxide (of average thickness around 500 nm) investigated in the present work have been deposited on amorphous silica substrates (MaTek, roughness ca 1 nm) by means of Radio Frequency (RF) magnetron sputtering starting from Cu metal target (American Elements). Table 1 summarizes the films prepared and considered in the present work, together with the deposition conditions.

Table 1. Sputtering conditions for the CuO films prepared.

T_{sub} (°C)	Rf power (W)	O_2 amount (%)	Total *P* (mbar)	Deposition time (min)
RT	200	25	4×10^{-2}	15
100	200	25	4×10^{-2}	15
200	200	25	4×10^{-2}	15
300	100	25	4×10^{-2}	15
300	200	25	4×10^{-2}	15
300	300	25	4×10^{-2}	15
300	200	15	4×10^{-2}	15
300	200	20	4×10^{-2}	15
300	200	30	4×10^{-2}	15
300	200	40	4×10^{-2}	15
300	200	50	4×10^{-2}	15
300	200	60	4×10^{-2}	15
300	200	70	4×10^{-2}	15
400	200	25	4×10^{-2}	15
500	200	25	4×10^{-2}	15
600	200	25	4×10^{-2}	15
700	200	25	4×10^{-2}	15

As can be appreciated from Table 1, the deposition conditions were selected in order to test the effect, on the final CuO films, of three different parameters that were changed separately by keeping all the other deposition conditions fixed: i) the substrate temperature, that was varied from

no-heating to 700°C; ii) the O_2 amount, varied from 15% to 70%; and, iii) the radio-frequency (RF) power that was set at 100, 200 and 300 W.

The structural properties of the deposited thin films were characterized by x-ray diffraction (XRD) by means of a Bruker D8 Advance instrument (Cu radiation).

Film morphology was analyzed by means of Atomic Force Microscopy (AFM) with an Autoprobe CP Research Microscope (Thermomicroscope-VEECO), operating in contact mode, by means of sharpened pyramidal silicon tip (curvature radius < 20 nm) onto rectangular microlevers (force constant, 0.03 N/m) (Thermomicroscope-VEECO). For each analyzed sample, scans of different areas were carried out with a scan rate in the range 0.7-1.0 Hz.

Photocatalytic experiments were carried out in a 250-mL pyrex discontinuous batch reactor with an external cooling jacket and equipped with connections for inlet/outlet of argon gas (15 mL/min), which serves as a mean of collection and transfer of gaseous products to the analysis system. The reactor was filled with a 1:1 water-methanol mixture. The supported CuO nanosystems were located on the internal walls of the photoreactor. The reactor was externally enveloped by an aluminum foil. All the experiments were carried out at 20°C. Gaseous products were analyzed by an Agilent HP 6890 Gas Cromatographic (GC) apparatus using a Molsieve 5A column, with Ar as the carrier gas. A thermal conductivity detector (TCD) was employed for H_2 quantification, whereas C-containing compounds were measured by a PoraPLOTQ column connected to a methanator and to a flame ionization detector (FID).A 125 W medium pressure mercury lamp (Helios Italquartz) with a pyrex immersion well was used for UV-visible excitation. The photon flux was measured by using a DeltaOHM radiometer HD2302.0. Accordingly to Lianos *et al.* [50], the approximate average incident radiation power on the photocatalyst was 129 mW.

Solar-to-Fuel Efficiencies (SFE) were calculated as:

$$SFE = \frac{\Phi_{H_2} \times \Delta H^0_{298K}}{S} \times 100 \quad (1)$$

where Φ_{H_2} is the H_2 flow produced by each sample (expressed in $mol \times s^{-1} \times cm^{-2}$), ΔH^0_{298K} is the combustion enthalpy of H_2 at 25 °C (285.8 $kJ \times mol^{-1}$) and S is the total incident solar irradiance (expressed in $W \times cm^{-2}$). The product $\Phi_{H_2} \times \Delta H^0_{298K}$ represents the energy stored in the produced hydrogen [51].

XPS data were collected with a ultra-high vacuum system equipped with a dual anode X-ray source and a Scienta R3000 analyser. The base pressure before starting the data collection was $2x10^{-10}$ mbar. The XPS system was properly calibrated following the method reported in Ref. [52]. The Al k_α line at $h\nu$=1486.7 eV was selected for all XPS measurements. The spectra were collected with a pass energy of 50 eV, yielding an overall energy resolution of 0.9 eV.

RESULTS

In the following sections are presented the results of the investigation carried out on the CuO thin films deposited under different experimental conditions. For sake of clarity, the results will be organized as a function of the deposition parameter varied during the growth of the CuO films.

Substrate Temperature Effect on Structure and Morphology

A first series of copper oxide thin films was grown by changing the substrate temperature from no-heating (indicated as RT) to 700°C (100, 200, 300, 400, 500, 600 and 700°C). As can be seen from Table 1, the other sputtering parameters were kept fixed (*i.e.*, total pressure = $4.3 \cdot 10^{-5}$ bar, Ar flux = 20 sccm, O_2 flux = 5 sccm, RF-power = 200 W). Deposition time was 15 minutes for all the films.

Figure 1 reports the x-ray diffraction (XRD) patterns for the series of thin films deposited as a function of increasing substrate temperature. Vertical red bars refer to the reference pattern for the monoclinic tenorite CuO phase.

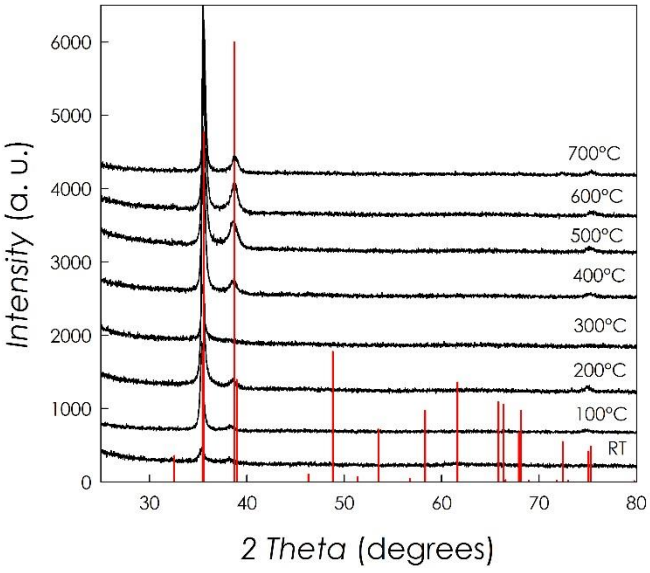

Fig. 1 – XRD patterns for the CuO thin films grown at different substrate temperatures. Vertical red bars refer to the reference pattern for the tenorite CuO.

From Figure 1 it is possible to observe that the CuO thin films are single-phase and their XRD patterns are consistent with the expected tenorite crystal structure. In addition, a significant orientation of the films is as well evident from the reported patterns where the strongest reflection around 35° corresponds to the (-111) Bragg peak. A second less intense peak (~38.5°) pertains to the (111) reflection which, however, should be the most intense reflection based on the calculated pattern (see vertical red bars). There is not a clear and simple dependence of the relative intensities of the two diffraction peaks observed as a function of the deposition temperature but it can be concluded that the deposited thin films are strongly oriented along the (-111) direction with a complete iso-orientation for the film deposited at 300°C. This peculiar growth direction has been also observed in previous reports [48, 49] on the RF-sputtering deposition of CuO thin films. However, Gosh et al. [48] could observe the formation of pure CuO only above 300°C (while at lower temperatures Cu_2O was the main phase) and Lim et al. found Cu-impurities in most of the deposited thin films, for similar deposition conditions [49].

In Figure 2 is reported the position of the peak around 35°, *i.e.*, the (-111) reflection, as a function of the substrate temperature during the CuO film deposition. Horizontal red line corresponds to the position of the (-111) reflection in bulk CuO.

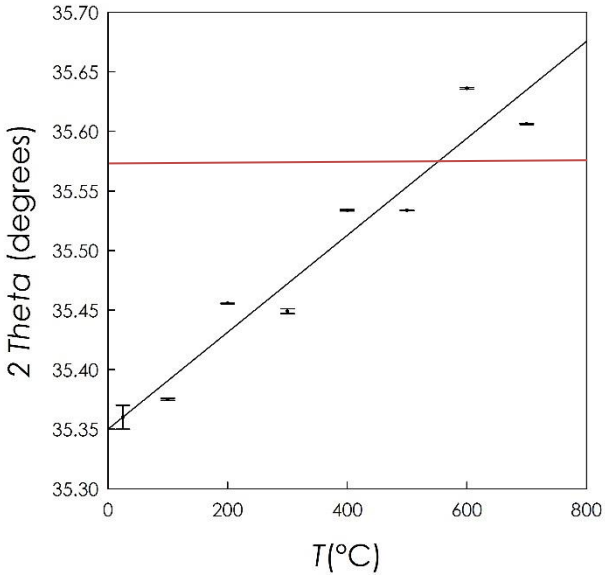

Fig. 2 – Position of the most intense peak in the patterns as a function of substrate temperature. Red line represents the CuO bulk value of the (-111) reflection.

From Figure 2 it is possible to observe a general progressive shift of the diffraction peak towards higher angles by increasing the substrate temperature; this in turn implies a progressive contraction of the unit cell by increasing *T*. This behavior could be correlated to both a partial change of Cu oxidation state (due, for example, to oxygen non-stoichiometry) and/or to microstructural effects such as lattice strain.

To probe the Cu oxidation state in the deposited CuO films, XPS measurements have been performed on the two samples deposited at the lowest (RT) and highest (700°C) substrate temperature. Figure 3 reports the Cu-2*p* and O-1*s* spectra for the above mentioned films.

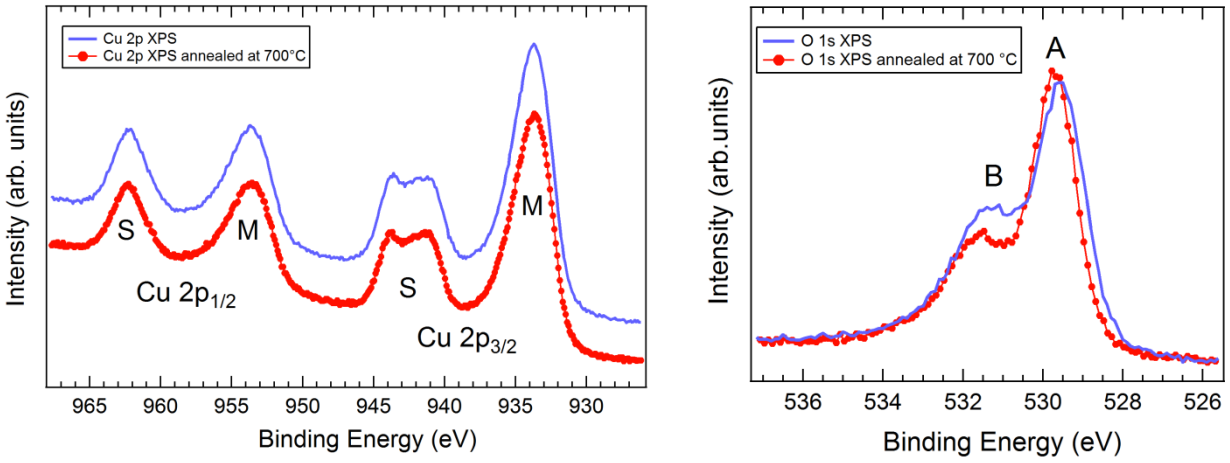

Fig. 3 – Cu-2p and O-1s spectra for the CuO thin films deposited with the substrate kept at RT and 700°C.

Peaks shape and position for the two films, which represent the lower and higher limit of the substrate temperature series, are very close each other, and the Cu-2*p* XPS spectra confirm that Cu is present in the +2 oxidation state. Indeed, the Cu 2p core lines show the spin-orbit split peaks in the 930-947 eV binding energy (BE) range for the Cu $2p_{3/2}$ component and in the 947-967 eV BE range for the Cu $2p_{1/2}$ component. Each spin orbit split contribution shows a main line (M) at lower BE and a satellite (S) at higher BE. These spectra are characteristic of the Cu^{2+} emission, being the main line mainly related to the charge-transfer screened $\underline{2p}3d^{10}\underline{L}$ final state of the Cu^{2+} cation and the satellite to the atomic-like $\underline{2p}3d^{9}$ unscreened final state, where $\underline{2p}$ indicates the 2p core-hole in the final state, and $\underline{L}$ the O 2p hole related to the O 2p → Cu 3d charge transfer effect [53]. Slight changes upon annealing seem to involve the O 1s emission only. The main line (A) at BE=529.5 eV width reduces upon annealing, and a reduction of the high BE shoulder (B) is observed after annealing. As this peak can be ascribed to the contribution of OH and O adsorbed [54] on the surface, we can conclude that annealing has partially contributed to reduce the species adsorbed on the surface.

As the electronic properties of Cu cations appear to be nearly identical from the surface sensitive XPS probe, if a change of oxidation state occurs as a function of the substrate temperature during deposition, this would be related to the bulk of the sample and not to the surface. However,

this result also suggests that the significant peak shift observed in the diffraction pattern could be to microstructural/relaxation effects.

All the thin films deposited as a function of substrate temperature underwent AFM investigation in order to define their surface morphology. The results for the 5 μm × 5 μm scans are reported in Figure 4.

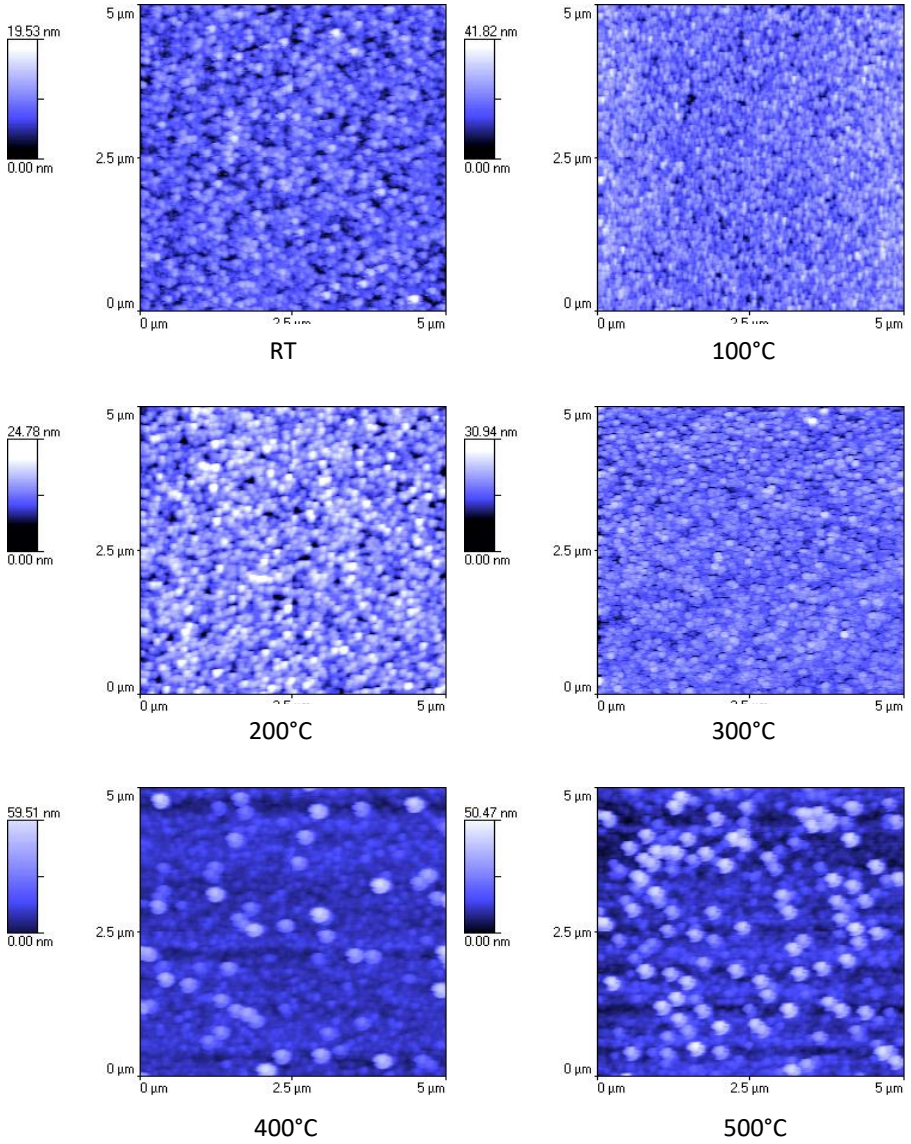

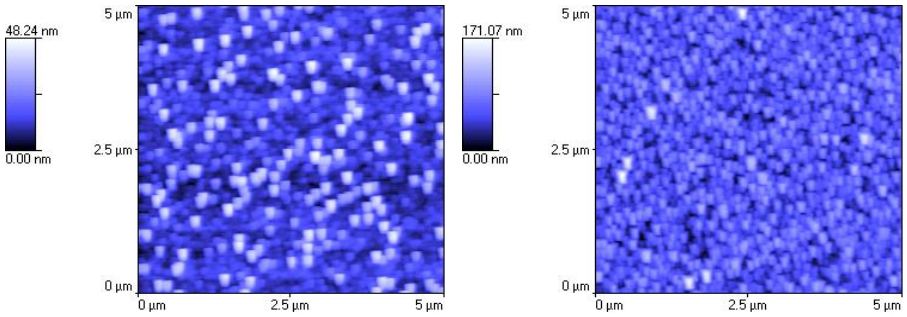

Fig. 4 – 5 µm × 5 µm AFM scans for the CuO thin films deposited at different substrate temperatures.

Overall, the AFM scans reveal the presence of nanosized grains with a nearly spherical shape for all the substrate temperatures. The average grain size (*e.s.d.* ±10 nm) and surface roughness (R_{rms}) calculated from the AFM scans are reported in Table 2.

Table 2 – Average grain size and surface roughness determined from the AFM scans for the CuO thin films deposited at different substrate temperatures.

Substrate Temperature (°C)	*Average Grain Size (nm)*	R_{rms} *(nm)*
RT	150	2.5(2)
100	160	4.1(1)
200	150	3.2(3)
300	110	3.1(6)
400	115	8.5(5)
500	220	8.6(2)
600	218	8.2(1)
700	220	20.7(5)

Root mean square surface roughness indicate very smooth films with a tendency of R_{rms} to increase with the substrate temperature. In general the roughness is below 10 nm for all the substrate temperatures except for the film deposited at 700°C where it reaches a value around 20 nm. Such R_{rms} values are in agreement with previous literature reporting AFM investigation for a limited set of substrate temperatures [46, 47]. The presence of a sharp roughening transition in the range 600°-700°C is compatible with a columnar growth mechanism, which is expected to hold for $T/T_m<0.5$ (where T is the substrate temperature and T_m is the melting temperature of the bulk material) [55-57].

In order to get some information on the films density and the growth mechanism, on some selected samples a SEM investigation has been performed. Figure 5 reports the SEM images (lateral section) for the CuO thin films grown with a substrate temperature of 300 and 600°C, as selected examples.

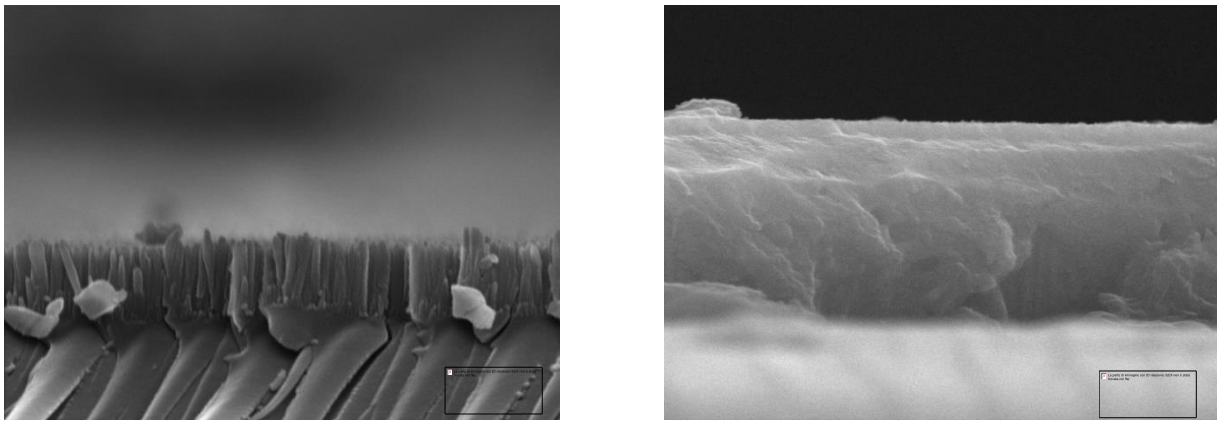

Fig. 5 – SEM images for the CuO thin films deposited at 300°C (left) and 600°C (right).

The SEM images suggest a columnar growth characterized by the presence of vertical well-aligned nanorods, which is more evident and clear for the CuO film deposited at 300°C while for the film deposited at 600°C clear nanorods are only seen in some parts of the sample. Also, the structure looks denser by increasing the substrate temperature as a consequence of the higher mobility of the adatoms on the film surface.

RF Power Effect on Structure and Morphology

A second series of copper oxide thin films was grown by changing the RF power from 100 W to 300 W (100, 200 and 300 W) while keeping fixed the following sputtering parameters: substrate temperature = 300°C, total pressure = $4.3 \cdot 10^{-5}$ bar, Ar flux = 20 sccm, O_2 flux = 5 sccm). Deposition time was 15 minutes for all the films.

Figure 6 reports the XRD patterns collected on the three films deposited at the three different RF power values.

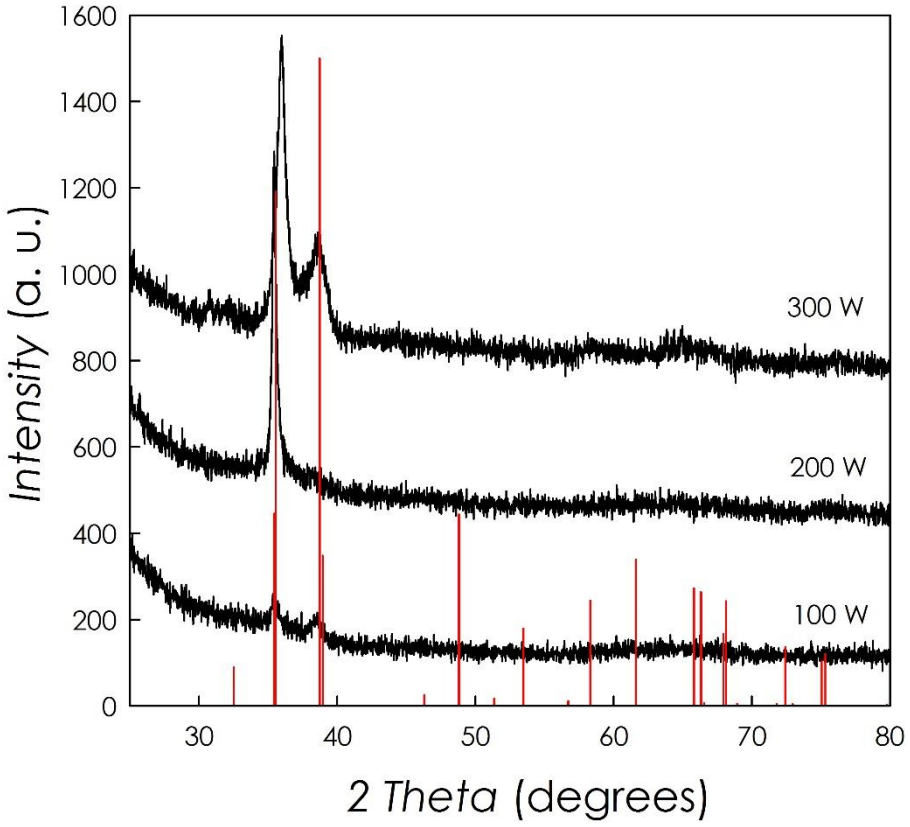

Fig. 6 – XRD patterns for the CuO thin films grown at different RF power values. Vertical red bars refer to the reference pattern for the tenorite CuO.

These results confirm that the thin films have been grown as single-phase materials at each RF power value and with the monoclinic tenorite crystal structure. As for the case of the thin films series grown at different substrate temperatures, a significant orientation of the films is as well evident from the reported patterns. From the diffraction data it was possible to observe a significant shift at higher angle of the main diffraction peak (the one located around 35°) passing from the films deposited at 100 and 200 W (ca. 35.45°) to the film deposited at 300 W (35.96°), thus suggesting a cell contraction. Lim et al. [45] reported the deposition of copper oxides thin films by means of RF sputtering employing analogous deposition conditions and by changing the RF power. With respect

to their results, where multi-phase films composed of CuO and Cu_2O were obtained, we could successfully grow single-phase CuO films.

AFM investigation of the deposited thin films is reported in Figure 7 showing a spherical-like shape for all the samples with a progressive increase of both grain size and roughness by increasing the RF power employed during the film deposition.

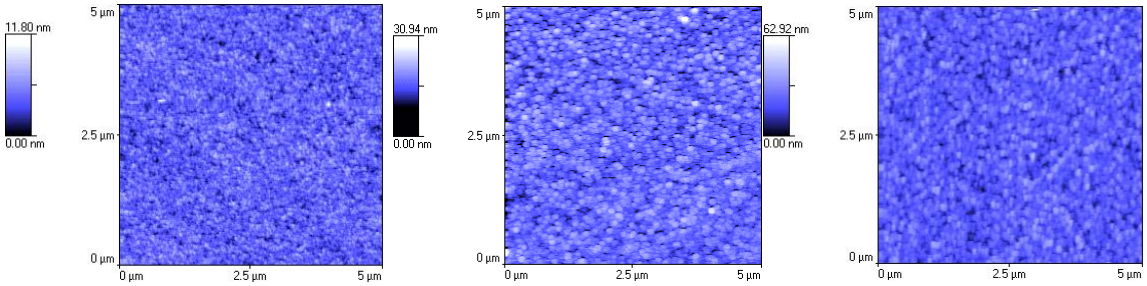

Fig. 7 – 5 µm × 5 µm AFM scans for the CuO thin films deposited at different RF power values.

The grain size and average surface roughness for the three thin films are shown in Figure 8.

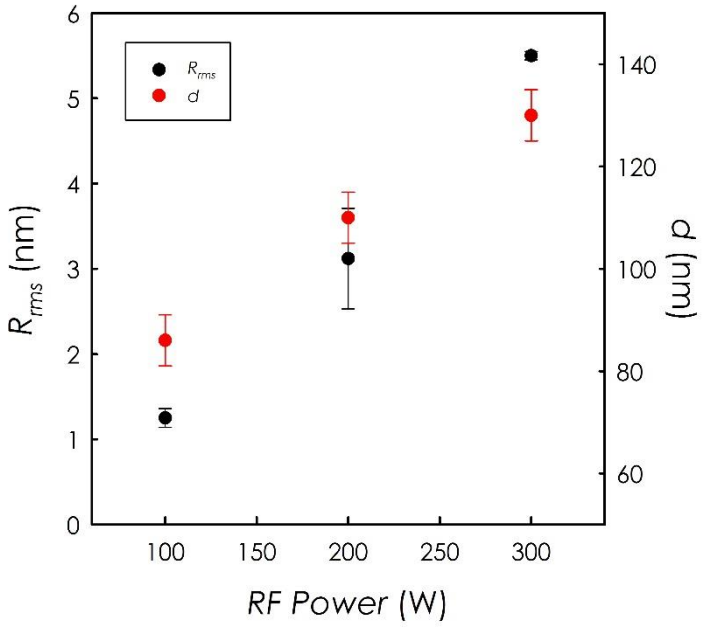

Fig. 8 – Trend of surface roughness and grain size for the CuO thin films deposited at different RF power values.

A clear trend is seen from Figure 8 with the average grain size and roughness increasing by increasing the RF power during thin films deposition. This is due to the fact that an increase in the RF power causes an increase in the energy of the Ar^+ ions when they collided with the target resulting in an increase in the surface mobility of the sputtered particles. The SEM investigation (not shown) reveals a clear columnar growth for the CuO films grown at lower RF power values while a denser and more compact lateral structure for the film deposited at 300 W.

Oxygen Content Effect on Structure and Morphology

The last series of CuO thin films was deposited by changing the oxygen content in the sputtering gas while keeping all the other parameters fixed (*i.e.*, substrate temperature = 300°C, total pressure = $4.3 \cdot 10^{-5}$ bar, RF power = 200 W). The list of the samples prepared is presented in Table 1. The amount of oxygen was changed from 15 to 70% relative to the total amount of O_2+Ar sputtering gas.

The effect of oxygen content variation on the thin films composition is shown in Figure 9 reporting the XRD patterns as a function of the O_2 percentage.

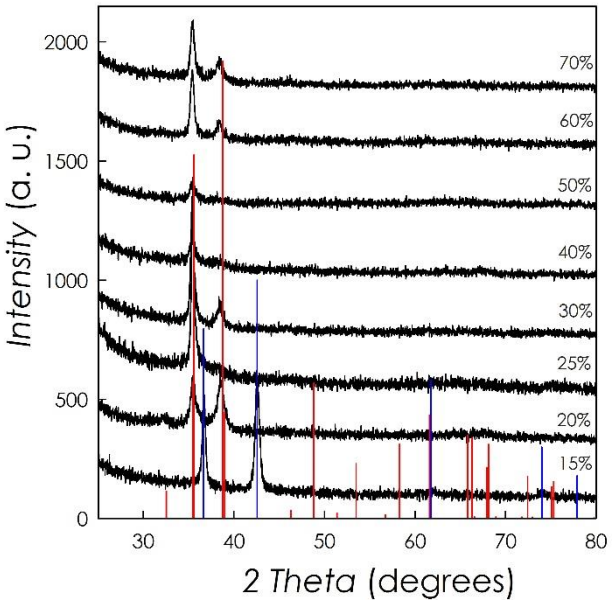

Fig. 9 – XRD patterns for the copper oxides thin films grown at different oxygen contents. Vertical red bars refer to the reference pattern for the tenorite CuO while vertical blue bars refer to the Cu_2O Bragg peaks.

From the inspection of the XRD patterns reported in Figure 9 it can be seen that when the oxygen amount is 15% in the sputtering gas mixture (O_2+Ar) the stable phase is Cu_2O, while for all the other oxygen contents single-phase tenorite CuO thin films are obtained. It is interesting to note that passing from 15% to 20% of O_2 amount we could selectively grow single phase Cu_2O and CuO, respectively, thus avoiding the formation of multi-phase thin films, as reported in literature [46]. An analysis of the position of the main peak of the CuO thin films (at about 35°) revealed a modest variation of the position along with the oxygen content, with all the peaks falling within 35.43±0.03. These are very small variations with respect to those observed by varying the substrate temperature or the RF power thus suggesting that the oxidation state of the copper ions in the CuO thin films is +2 already at the lowest oxygen content stabilizing the CuO phase. This is also in agreement with the XPS data reported in the previous section.

Some selected AFM images of the deposited thin films are shown in the following Figure.

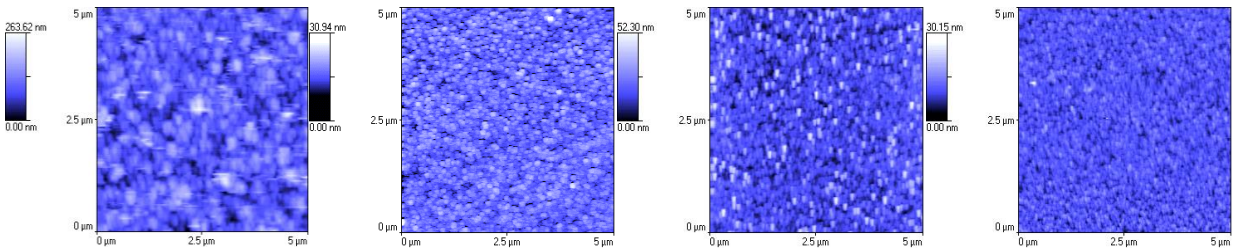

Fig. 10 – 5 µm × 5 µm AFM scans for the copper oxides thin films deposited at different oxygen contents. From left to right: 15, 25, 40 and 50%.

Average roughness of the CuO thin films are in the range of 3-6 nm while the Cu_2O (first image in Figure 10) has a significant higher R_{rms} of the order of 36.1(6) nm. In addition, while the average grain size of the three CuO thin films is within 100-150 nm (in agreement with the data shown previously), the grains of the Cu_2O are significantly larger, falling between 250 and 300 nm.

SEM inspection (not shown) revealed a clear columnar growth up to 40% of oxygen content, while at higher concentrations the films look less well-defined in their lateral section and with a higher density.

Photocatalytic Activity

After the extensive study of the correlation between the deposition conditions and the structural and morphological properties of the nanostructured thin films grown, an investigation on the photocatalytic activity has been carried out. This was performed on selected CuO thin films according to preliminary consideration relative to the morphology, density, grain size and crystal structure in order to shed light on the most important characteristics affecting the photocatalytic properties. All the measurements have been performed as described in the Experimental section by using a 1:1 water:methanol solution under irradiation with a conventional medium pressure Hg lamp. Photoreforming reactions have been carried out for 20 h in order to verify the materials stability as well.

Recently, the production of hydrogen has been extended to the photodecomposition of methanol (CH_3OH), which has a lower splitting energy than water. Sakata et al. [58-61] have described that the reaction can proceed either stepwise, involving stable intermediates such aldehydes and acids (Eqs. (1) and (3)).

$$CH_3OH\ (l) \longrightarrow HCHO\ (g) + H_2\ (g) \qquad DG^0_1 = 64.1\ kJ\ mol^{-1} \qquad (1)$$

$$HCHO\ (g) + H_2O\ (l) \longrightarrow HCOOH\ (l) + H_2\ (g) \qquad DG^0_2 = 47.8\ kJ\ mol^{-1} \qquad (2)$$

$$HCOOH\ (l) \longrightarrow CO_2\ (g) + H_2\ (g) \qquad DG^0_3 = 95.8\ kJ\ mol^{-1} \qquad (3)$$

One step on the catalyst surface to give the overall reaction (Eq. (4)) has been reported by Chen et al. [62].

$$CH_3OH\ (l) + H_2O\ (l) \longrightarrow CO_2\ (g) + 3H_2\ (g) \qquad DG^0 = 16.1\ kJ\ mol^{-1} \qquad (4)$$

Hydrogen is produced in all of these steps. The water splitting reaction is endothermic and requires an input energy of 237 kJ/mol [63]. Methanol has a lower splitting energy relative to water. In Figure 11 a possible scheme of reactions, based on the literature [63, 64], is estimated in order to better understand the photocatalytic process of hydrogen formation from the aqueous methanol solution. The overall process can be divided into three steps. In the first step (Eqs. (5) and (7)), there exists a water-splitting process on the surface of CuO photocatalyst. The rate of water splitting is limited by accumulation of active photogenerated holes and, OH radicals. In second step (Eqs. (8) and (11)), the photogenerated holes attack methanol to form formaldehyde, which are further oxidized by both ,OH radicals and photogenerated holes to produce formic acid [65]. At third step (Eqs. (12) and (14)), the formic acid is decarboxylated by the photo-Kolbe reaction to release CO_2 [66]. The H^+ deprotonated during whole process transfers to the loaded CuO particles and then reduce to hydrogen by the photogenerated electrons. However, actual mechanism must be more complicated, which relies on monitoring reactants, intermediates, products as well as radicals. Further investigations with the help of advanced instruments and in situ techniques are needed.

Step 1

$$CuO \xrightarrow{h\nu} e^-_{(CuO)} + h^+_{(CuO)} \quad (5)$$

$$h^+ + H_2O \longrightarrow H^+ + \bullet OH \quad (6)$$

$$2H^+ + 2e^- \xrightarrow[CuO]{} H_2 \quad (7)$$

Step 2

$$CH_3OH + h^+ \longrightarrow \bullet CH_2OH + H^+ \quad (8)$$

$$\bullet CH_2OH + h^+ \longrightarrow HCHO + H^+ \quad (9)$$

$$2H^+ + 2e^- \xrightarrow[CuO]{} H_2 \quad (10)$$

$$HCHO + \bullet OH + h^+ \longrightarrow H^+ + HCOOH \quad (11)$$

Step 3

$$HCOOH \longrightarrow HCOO^- + H^+ \quad (12)$$

$$HCOO^- + 2h^+ \longrightarrow H^+ + CO_2 \quad (13)$$

$$2H^+ + 2e^- \xrightarrow[CuO]{} H_2 \quad (14)$$

Fig. 11– Photocatalytic reaction for hydrogen production from aqueous methanol solution in the proposed mechanism

The CuO nanostructured thin films, which underwent the photocatalytic test, are reported in the following table.

Table 3 – Deposition parameters for the CuO thin films which underwent photocatalytic activity study

Sample	T_{sub} (°C)	Rf power (W)	O_2 amount (%)
1	RT	200	25
2	300	200	25
3	600	200	25
4	300	200	40
5	300	200	60
6	RT	100	25

Such selection of deposition conditions allowed to test the dependence of one single parameter at time on the catalytic properties: substrate temperature (RT, 300 and 600°C); oxygen content in the sputtering gas (25, 40 and 60%) and RF power value (200 and 100 W).

In addition, a replica of sample 2 (indicated as sample 7) was prepared followed by a further deposition of Ag nanoparticles (performed at RT by means of RF-magnetron sputtering starting form an Ag target) in order to increase the absorption in the visible spectral range and to improve the photocatalytic properties, as discussed in the previous sections. The Ag nanoparticles were deposited in form of isolated "islands" of tens of nanometers after the growth of the CuO films.

Figure 12 reports the H_2 evolution for all the CuO thin films tested and listed in Table 3. The data are normalized to the geometrical surface area of the samples.

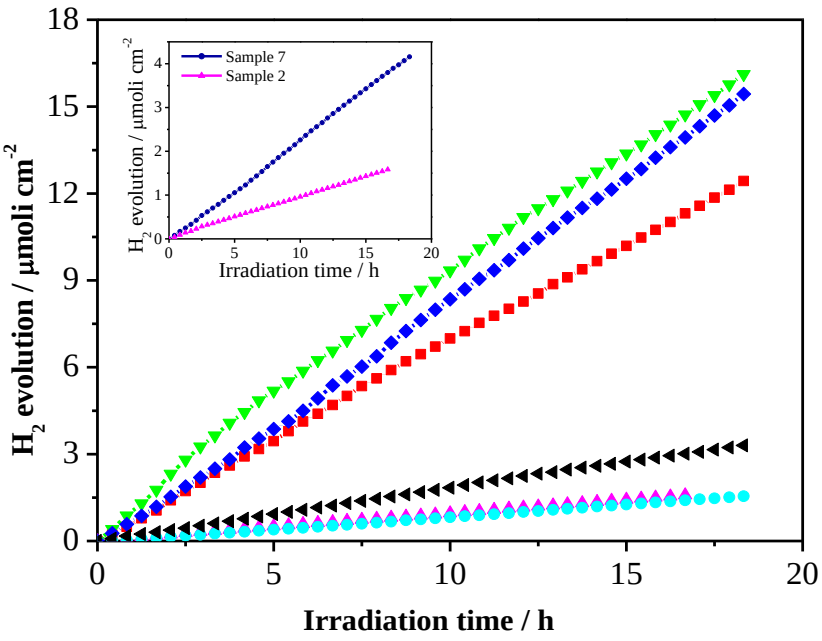

Fig. 12 – Hydrogen production as a function of time in photocatalytic experiments of methanol photo-dehydrogenation over CuO nanostructured thin film: Sample 1 (■)Sample 2 (▲) Sample 3 (●) Sample 4 (▼) Sample 5 (◆)Sample 6 (◄) In the inset the effect on photocatalytic activity of the functionalization with Ag-NPs Sample 7 (●).

.

The constant hydrogen production observed in Figure 12 suggests that all the CuO thin films tested are stable during the irradiation time (20 hrs). This is also confirmed by the visual inspection

of the samples after the photocatalytic experiments showing no appreciable photocorrosion of the CuO layer, which is a potential problem for Cu based systems [67, 68]. Among the best performing samples, in terms of hydrogen evolution, it is possible to find sample 4 of Table 3, *i.e*. the one deposited at intermediate oxygen content among sample 2 (25%) and 5 (60%). With respect to these last two samples the H_2 evolution is significantly higher. As described in the pertinent section above, the grain size and nanostructure is very similar for the three thin films deposited at varying oxygen content. A more dense film is obtained at 60% of O_2 content with a less defined columnar growth which may explain the lover H_2 evolution for this sample. However, such difference is not found between the 25% and 40% films. The only significant difference between these two samples, that could account for the observed performances, is the higher level of iso-orientation, inferred from the XRD patterns of Figure 9, found for the CuO film grown at 40% of oxygen content. Such preferential growth may led to a greater activity related to the crystallographic plane exposed (-111).

Regarding the samples deposited at different substrate temperatures, that have been tested relative to the photocatalytic performance, the CuO film grown without substrate heating (n° 1) shows the best performance with respect to the samples grown at 300 and 600°C (samples n° 2 and 3, respectively). In this case, according to the investigation reported in the pertinent section, the low grain size, coupled to a better defined morphology of the nanostructure (characterized by aligned nanorods) and to a lower density results in a more efficient H_2 production. However, the nearly 10-fold improvement of the H_2 production for sample 1 with respect to sample 2 (grown in the same conditions but heating the substrate at 300°C), which have no drastic differences in terms of morphology, may also be correlated to the structural properties reported in Figure 2. From the analysis of the XRD patterns we could observe an expansion of the lattice by reducing the substrate temperature during deposition, with the lowest position of the main peak (and thus bigger lattice) found for the CuO film grown at RT. Such expansion of the cell may be due to the presence of partially reduced Cu ions leading to an improvement of the catalytic activity.

The last CuO nanostructured thin film with an enhanced photocatalytic activity is a sample similar to the previous film (n° 1) but deposited at a lower RF power value of 100 W. This film shows a further enhanced H_2 production with respect to the film deposited at 200 W (and with the same remaining deposition parameters). As presented in Figure 8, by lowering the RF power the CuO film grows with a smaller grain size which is expected to improve the catalytic reaction with the sacrificial agent. Since the application of BET method is not trivial due to the impossibility to remove the cupper oxides films from the supporting substrate without altering their nature and due to the unavoidable and not negligible contribution of the substrate, an estimation of the surface area of the thin films has been done by means of AFM. Consistently with the morphology described in the previous section, relatively small values in the range 0.4-0.5 m^2/g where obtained, with no significant difference between the samples. This clearly indicates that surface area effects can be excluded. While the activity trend is scientifically interesting, the absolute Solar-to-Fuel efficiency are modest and varies from 0.02 to 0.07 % for the less to the most active sample. These compact supported CuO materials are less active with respect to more reactive branched nanowires CuO structures [69] where, under similar working conditions, an H_2 evolution of about 3 L h^{-1} m^{-2} where observed, which is nearly one order of magnitude higher than the 0.4 L_{H2} h^{-1} m^{-2} observed for the present best sample. This observation strongly highlights the importance of open nanostructure in driving both photo-activity and stability/resistance against mechanical stresses induced by the formation of hydrogen bubbles. However, it should be remarked that the photo-activity of the nanostructured thin films reported here, prepared by means of sputtering, while not yet optimal, is a very appealing starting point within the framework of a cost-effective and scalable method.

Finally, an interesting comparison can be done for films n° 2 and 7 which have been grown under the same conditions but further functionalizing film n° 7 with Ag nanoparticles. As can be seen from Figure 12, the H_2 evolution has been improved of about 4 times in the film where Ag

nanoparticles were present. Similar beneficial effects due to the presence of Ag were previously reported [70, 71].

CONCLUSIONS

In this paper we have carried out an extensive study relative to the deposition of CuO thin films by means of RF-magnetron sputtering starting from a Cu metal target and varying (once at time) three deposition parameters: i) substrate temperature; ii) RF-power, and iii) oxygen content in the sputtering gas. All the films deposited were single phase materials of tenorite CuO except for the lowest oxygen partial pressure used in the depositions which led to the growth of single phase Cu_2O.

The extensive structural, morphological, and photocatalytic activity characterization allowed to put in prominence the parameters that seems to mostly affect the catalytic properties of CuO films. In particular, even though all the deposited films show a nanostructure composed of nanorods of variable diameter between 80 and 200 nm, those conditions that lead to the growth of well aligned rods, *i.e*. relatively low substrate temperatures and from low to intermediate oxygen partial pressures, resulted in more efficient catalytic activities. It is also clear that a reduction in the diameter of the rod down to 100 nm improves the photocatalysis and this effect seems to be more relevant than the variation of the film roughness. Finally, our investigation suggests a relevant role of the crystallographic orientation of the CuO tenorite film on the catalytic activity, as demonstrated by the significant improvement in the H_2 evolution for highly oriented films. Within the framework of the films and parameters investigated in this work, the relevance of the proper choice of the growth conditions is very significant, with photocatalytic activity improvements of more than 10 times for the best performing nanostructured films with respect to the less active samples. Finally, it should be stressed that the photo-activity results reported here are related to films grown with a cost-effective

and scalable process which can open the way to real large-scale applications. Further work is planned in order to improve the photocatalytic activity of RF-sputtered CuO thin films.

Moreover, since the photocatalytic mechanism of most metal oxides used in the photoreforming reaction is similar, the guidelines unveiled in this work might be extended to other systems thus providing a guide to grow more efficient metal oxides nanostructured thin films.

ACKNOWLEDGEMENTS

This work was supported through the INSTM-RL “ATLANTE” project.

REFERENCES

[1] Zinoviev, S.; Muller-Langer, F.; Das, P.; Bertero, N.; Fornasiero, P.; Kaltschmitt, M.; Centi, G.; Miertus, S. Next-generation biofuels: Survey of emerging technologies and sustainability issues, *ChemSusChem* **2010**, *3*, 1106-1133.

[2] Walter, M. G.; Warren, E. L.; McKone, J. R.; Boettcher, S. W.; Mi, Q.; Santori E. A.; Lewis, N. S. Solar water splitting cells. *Chem. Rev.* **2010**, *110*, 6446–6473

[3] Chen, X.; Shen, S.; Guo L.; Mao, S. S. Semiconductor-based photocatalytic hydrogen generation. *Chem. Rev*. **2010**, *110*, 6503–6570

[4] Fujishima, A.; Honda, K. Electrochemical Photolysis of water at a semiconductor electrode. *Nature*, **1972**, *238*, 37–38

[5] Barreca, D.; Carraro, G.; Gombac, V.; Gasparotto, A.; Maccato, C.; Fornasiero, P.; Tondello, E. Supported metal oxide nanosystems for hydrogen photogeneration: quo vadis? *Adv. Funct. Mater*. **2011**, *21*, 2611-2623.

[6] Cristino, W.; Caramori, S.; Argazzi, R.; Meda, L.; Marra G. L.; Bignozzi, C. A. Efficient photoelectrochemical water splitting by anodically grown WO3 electrodes. *Langmuir*, **2011**, *27*, 7276–7284

[7] Cole, B.; Marsen, B.; Miller, E.; Yan, Y.; To, B.; Jones K.; Al-Jassim M. Evaluation of nitrogen doping of tungsten oxide for photoelectrochemical water splitting. *J. Phys. Chem. C*, **2008**, *112*, 5213–5220

[8] Hu, Y. S.; Kleiman-Shwarsctein, A.; Forman, A. J.; Hazen, D.; Park J. N.; McFarland, E. W. Pt-Doped α-Fe_2O_3 thin films active for photoelectrochemical water splitting. *Chem. Mater*. **2008**, *20*, 3803–3805

[9] Zhong, D. K.; Sun, J.; Inumaru H.; Gamelin, D. R.; Solar water oxidation by composite catalyst/α-Fe_2O_3 photoanodes. *J. Am. Chem. Soc*., **2009**, *131*, 6086–6087

[10] Carraro, G.; Maccato, C.; Gasparotto, A.; Montini, T.; Turner, S.; Lebedev, O. I.; Gombac, V.; Adami, G.; Van Tendeloo, G.; Barreca, D.; Fornasiero, P. Enhanced hydrogen production by photorefoming of renewable oxygenates through nanostructured α-Fe_2O_3 polymorphs. *Adv. Funct. Mater*. **2014**, *24*, 372-378.

[11] Barreca, D.; Fornasiero, P.; Gasparotto, A.; Gombac, V.; Maccato, C.; Montini, T.; Tondello, E.; The potential of supported Cu_2O and CuO nanosystems in photocatalytic H_2 production. *ChemSusChem*, **2009**, *2*, 230-233.

[12] Hu, C. –C.; Nian, J. –N.; Teng, H. Electrodeposited p-type Cu_2O as photocatalyst for H_2 reduction in the presence of WO_3. *Sol. Energy Mater. Sol. Cells*, **2008**, *92*, 1071-1076.

[13] Nian, J. –N.; Hu, C. –C.; Teng, H. Electrodeposited p-type Cu_2O for H_2 evolution from photoelectrolysis of water under visible light illumination. *Int. J. Hydrogen Energy*, **2008**, *33*, 2897-2903.

[14] Kim, T. W.; Ha, H. –W.; Paek, M. –J.; Hyun, S. –H.; Choy, J. –H.; Hwang, S. –J. Unique phase transformation behavior and visible light photocatalytic activity of titanium oxide hybridized with copper oxide. *J. Mater. Chem*. **2010**, *20*, 3238-3245.

[15] Zhengbo, J.; Tao, C.; Jinyan, X.; Lu, G.; Ye, J.; Bi, Y.; Visible-ight-driven photoelectrochemical and photocatalytic performances of Cr-doped $SrTiO_3/TiO_2$ heterostructured nanotube arrays. *Sci. Reports* **2013**, *3*, 2720.

[16] Li, Y.; Zhang, L.; Torres-Pardo, A.; Gonzales-Calbet, J. M.; Ma, Y.; Oleynikov, P.; Terasaki, O.; Asahina, S.; Shima, M.; Cha, D.; Zhao, L.; Takanabe, K.; Kubota, J.; Domen, K.; Cobalt phosphate-modified barium-doped tantalum nitride nanorod photoanode with 1.5% solar energy conversion efficiency. *Nature Commun.*, **2013**, *4*, 2566.

[17] Garcia-Esparza, A. T.; Cha, D.; Ou, Y.; Kubota, J.; Domen, K.; Takanabe, K. Tungsten carbide nanoparticles as efficient cocatalysts for photocatalytic overall water splitting. *ChemSusChem*, **2013**, *6*, 168-181.

[18] Takanabe, K.; Domen, K. Preparation of Inorganic photocatalytic materials for overall water splitting. *ChemCatChem*, **2012**, *4*, 1485-1497.

[19] Kondarides, D. I.; Daskalaki, V. M.; Patsoura, A.; Verykios, X. E. Hydrogen production by photo-induced reforming of biomass components and derivatives at ambient conditions. *Catal. Lett*. **2008**, *122*, 26-35.

[20] Bowker, M. Photocatalytic hydrogen production and oxygenate photoreforming. *Catal. Lett*. **2012**, *142*, 923-929.

[21] Fu, X.; Long, J.; Wang, X.; Leung, D. T. C.; Ding, Z.; Wu, L.; Zhang, Z.; Li, Z.; Fu, X.; Photocatalytic reforming of biomass: A systematic study of hydrogen evolution from glucose solution. *Int. J. Hydrogen Energy*, **2008**, *33*, 6484-6491.

[22] Pham, T. V.; Rao, M.; Andreasson, P.; Peng, Y.; Wang, J.; Jinesh, K. B. Photocarrier generation in Cu_xO thin films deposited by radio frequency sputtering. *Appl. Phys. Lett*. **2013**, *102*, 032101.

[23] Mittiga, A.; Salza, E.; Sarto, F.; Tucci, M.; Vasanthi, R. Heterojunction solar cell with 2% efficiency based on a Cu_2O substrate. *Appl. Phys. Lett*., **2006**, *88*, 163502.

[24] Ray, S. C. Preparation of copper oxide thin film by the sol-gel-like dip technique and study of their structural and optical properties. *Sol. Energy Mater. Sol. Cells*, **2001**, *68*, 307-312.

[25] Ogwu, A. A.; Bouquerel, E.; Ademosu, O.; Moh, S.; Crossan, E.; Placido, F. The influence of rf power and oxygen flow rate during deposition on the optical trasmittance of copper oxide thin films prepared by reactive magnetron sputtering. *J. Phys. D: Appl. Phys*. **2005**, *38*, 266-271.

[26] Pierson, J. F.; Thobor-Keck, A.; Billard, A. Cuprite, paramelaconite and tenorite films deposited by reactive magnetron sputtering. *Appl. Surf. Sci*., **2003**, *210*, 359-367.

[27] Marabelli, F.; Parravicini, G. B.; Salghetti-Drioli, F. Optical gap of CuO. *Phys. Rev. B*, **1995**, *52*, 1433-1436.

[28] Siripala, W.; Ivanovskaya, A.; Jaramillo, T. F.; Baeck S. H.; McFarland, E. W. A Cu_2O/heterojunction thin film cathode for photoelectocatalysis. *Sol. Energy Mater. Sol. Cells*, **2003**, *77*, 229-237

[29] Jin, Z.; Zhang, X.; Li, Y.; Li, S.; Lu, G. 5.1% apparent quantum efficiency for stable hydrogen generation over eosin-sensitized CuO/TiO_2 photocatalyst under visible light irradiation. *Catal. Commun*. **2007**, *8*, 1267-1273.

[30] Choi, H. –J.; Kang, M. Hydrogen production from methanol/water decomposition in a liquid photosystem using the anatase structure of Cu loaded TiO_2. *Int. J. Hydrogen Energy* **2007**, *32*, 3841-3848.

[31] Gombac, V.; Sordelli, L.; Montini, T.; Delgado, J. J.; Adamski, A.; Adami, G.; Cargnello, M.; Bernal, S.; Fornasiero, P. CuO_x-TiO_2 photocatalysts for H_2 production from ethanol and glycerol solutions. *J. Phys. Chem. A*, **2010**, *114*, 3916-3925.

[32] Senevirathna, M. K. I.; Pitigala, P. K. D. D. P.; Tennakone, K. Water photoreduction with Cu_2O quantum dots on TiO_2 nano-particles. *J. Photochem. Photobiol. A*, **2005**, *171*, 257-259.

[33] Zhang, Z.; Wang, P. Highly stable copper oxide composite as an effective photocathode for water splitting via a facile electrochemical synthesis strategy. *J. Mater. Chem*., **2012**, *22*, 2456-2464.

[34] Zhang, Q.; Zhang, K.; Xu, D.; Yang, G.; Huang, H.; Nie, F.; Liu, C.; Yang, S. CuO nanostructures: Synthesis, characterization, growth mechanisms, fundamental properties, and aplications. *Progress in Mater. Sciences*, **2014**, *60*, 208-337.

[35] Maruyama, T. Copper oxide thin films prepared by chemical vapor deposition from copper dipicaloylmethanate. *Sol. Energy Mater. Sol. Cells*, **1998**, *56*, 85-92.

[36] Morales, J.; Sanchez, L.; Martin, F.; Ramos-Barrado, J. R.; Sanchez, M. Use of low-temperature nanostructured CuO thin films deposited by spray-pyrolisis in lithium cells. *Thin Solid Films*, **2005**, *474*, 133-140.

[37] Chen, L.; Shet, S.; Tang, H.; Wang, H.; Deutsch, T.; Yan, Y.; Turner J.; Al-Jassim, M. Electrochemical deposition of copper oxide nanowires for photoelectrochemical applications. *J. Mater. Chem*., **2010**, *20*, 6962–6967.

[38] Liu X. M.; Zhou, J. C.; Electrochemical deposition and characterization of Cu_2O nanowires. *Appl. Phys. A: Mater. Sci. Process*., **2005**, *81*, 685–689.

[39] Le, M.; Ren, M.; Zhang, Z.; Sprunger, P. T.; Kurtz R. L.; Flake, J. C. Electrochemical reduction of CO_2 to CH_3OH at copper oxide surfaces. *J. Electrochem. Soc*., **2011**, *158*, E45–E49.

[40] Singh, D. P.; Neti, N. R.; Sinha A. S. K.; Srivastava, O. N. Growth of different nanostructures of Cu_2O (nanothreads, nanowires and nanocubes) by simple electrolysis based oxidation of copper. *J. Phys. Chem. C*, **2007**, *111*, 1638–1645.

[41] Becerra, J. C.; Salvarezza R. C.; Arvia, A.J. The influence of slow $Cu(OH)_2$ phase formation on the electrochemical behaviour of copper in alkaline solutions. *Electrochim. Acta*, **1988**, *33*, 613–621

[42] Pham, T. V.; Rao, M.; Andreasson, P.; Peng, Y.; Wang, J.; Jinesh, K. B. Photocarrier generation in Cu_xO thin films deposited by radio frequency sputtering. *Appl. Phys. Lett*. **2013**, *102*, 032101.

[43] Kumar, S. K.; Murugesan, S.; Suresh, S.; Raj, S. P. Nanostructured CuO thin films prepared through sputtering for solar selective absorbers. *J. Solar Energy*, **2013**, *2013*, 147270.

[44] Elfadill, N. G.; Hasim, M. R.; Chahrour, K. M.; Qaeed, M. A.; Chunsheng, W. The influence of oxygen pressure on the growth of CuO nanostructures prepared by RF reactive magnetron sputtering. *J. Mater. Sci: Mater. Electron*. **2014**, *25*, 262-266.

[45] Lim, K.; Park, J.; Kim, D. -G.; Kim, J. –K.; Kang, J. -W.; Kang, Y. –C. Rf Power dependence on the chemical and structural properties of copper oxide thin films obtained at various oxygen fractions. *Appl. Surf. Sci*., **2012**, *258*, 9054-9057.

[46] Prasad Reddy, M. H.; Pierson, J. F.; Uthanna, S. Structural, surface morphological, and optical properties of nanocrystalline Cu_2O and CuO films formed by RF magnetron sputtering: Oxygen partial pressure effect. *Phys. Status Solidi A*, **2012**, *209*, 1279-1286.

[47] Pham, T. V.; Rao, M.; Andreasson, P.; Peng, Y.; Wang, J.; Jinesh, K. B. Photocarrier generation in Cu_xO thin films deposited by radio frequency sputtering. *Appl. Phys. Lett.* **2013**, *102*, 032101.

[48] Ghosh, S.; Avasthi, D. K.; Shah, P.; Ganesan, V.; Gupta, A.; Sarangi, D.; Bhattacharaya, R.; Assmann, W. Deposition of thin films of different oxides of copper by RF reactive sputtering and their characterization. *Vacuum*, **2000**, *57*, 377-385.

[49] Lim, K.; Park, J.; Kim, D. -G.; Kim, J. –K.; Kang, J. -W.; Kang, Y. –C. Rf Power dependence on the chemical and structural properties of copper oxide thin films obtained at various oxygen fractions. *Appl. Surf. Sci*., **2012**, *258*, 9054-9057.

[50] Strataki, N.; Bekiari, V.; Kondarides, D. I. ; Lianos, P. Hydrogen production by photocatalytic alcohol reforming employing highly efficient nanocrystalline titania films. *App. Catal., B.* **2007**, *77*, 184-189.

[51] Reece, S. Y.; Hamel, Sung, K.; Jarvi, T. D.; Esswein, A. J.; Pijpers, J. J. H.; Nocera, D. C. Wireless solar water splitting using silicon-based semiconductors and earth-abundant catalysts. *Science*, **2011**, *334*, 645-648.

[52] Drera, G.; Salvinelli, G.; Åhlund, J.; Karlsson, P. G.; Wannberg, B.; Magnano, E.; Nappini, S.; Sangaletti, L. Transmission function calibration of an angular resolved analyser for X-ray photoemission spectroscopy: theory vs experiment. *J. Electron Spectrosc. Relat. Phenom*.**, 2014**, *195*, 109-116.

[53] a) Marder, M. P. *Condensed Matter Physics*, 2nd Edition, Wiley, 2010, Par.23.6.3 and Refs. therein; b) Parmigiani F.; Sangaletti, L. The Cu2p X-ray photoelectron core-lines in copper oxide based high temperature superconductors. *J. Electron Spectrosc. Relat. Phenom*. **1994**, *66*, 223-239.

[54] a) Platzman, I.; Brener, R.; Haick, H.; Tannebaum, R. Oxidation of polycrystalline copper thin films at ambient conditions. *J. Phys. Chem. C*, **2008**, *112*, 1101; b) Park, J.; Lim, K.; Ramsier, R. D.; Kang, Y. –C. Spectroscopic and morphological investigation of copper oxide thin films

prepared by magnetron sputtering at various oxygen ratios. *Bull. Korean Chem. Soc*., **2011**, *32*, 3395-3399.

[55] Thornton, J. A.; The microstructure of sputter deposited coatings *J. Vac. Sci. Technol. A*, **1986**, *4*, 3059-3065.

[56] Messier, R.; Ross, R. C. Evolution of microstructure in amorphous hydrogenated silicon. *J. Appl. Phys.*, **1982**, *53*, 6220-6225.

[57] Quartarone, E.; Mustarelli, P.; Grandi, S.; Marabelli, F.; Bontempi, E. Effects of the deposition parameters on the growth of ultrathin and thin SiO_2 films. *J. Vac. Sci. Technol A.* **2007**, *25*, 485-491.

[58] Kawai, T.; Sakata, T. Photocatalytic hydrogen production from liquid methanol and water *J. C. S. Chem. Comm.* **1980**, 15, 694-695.

[59] Kawai, T.; Sakata, T., Photocatalytic decomposition of gaseous water over TiO_2 and TiO_2-RuO_2 surfaces. *Chem. Lett.*, **1981**, *10*, 81-84.

[60] Sakata, T.; Kawai, Y. Heterogeneous photocatalytic production of hydrogen and methane from ethanol and water. *Chem. Phys. Lett*., **1981**, *80*, 341-344.

[61] Sakata, T.; Kawai, T.; Hashimoto, K. Photochemical diode model of Pt/TiO_2 particle and its photocatalytic activity. *Chem. Phys. Lett*., **1982**, *88*, 50-54.

[62] Chen, J.; Ollis, D. F.; Rulkens, W. H.; Bruning, H. Photocatalyzed oxidation of alcohols and organochlorides in the presence of native TiO_2 and metallized TiO_2 suspensions. Part (II): photocatalytic mechanisms. *Water Research*, **1999**, *33*, 669-676.

[63] Choi, H. –J.; Kang, M. Hydrogen production from methanol/water decomposition in a liquid photosystem using the anatase structure of Cu loaded TiO_2. *Int. J. Hydrogen Energy* **2007**, *32*, 3841-3848.

[64] Yoong, L. S.; Chong, F. K.; Dutta, B. K. Development of copper-doped TiO_2 photocatalyst for hydrogen production under visible light. *Energy*, **2009**, *34*, 1652-1661.

[65] Chen, T.; Feng, Z. C.; Wu, G. P.; Shi, J. Y.; Ma, G. J.; Ying, P. L. Mechanistic studies of photocatalytic reaction of methanol for hydrogen production on Pt/TiO_2 by in situ fourier transform IR and time-resolved IR spectroscopy. *J. Phys. Chem*. **2007**, *111*, 8005-8014.

[66] Chen, T.; Wu, G. P.; Feng, Z. C.; Hu, G. S.; Su, W. G.; Ying, P. L.; Li C. In situ FT-IR study of photocatalytic decomposition of formic acid to hydrogen on Pt/TiO_2 catalyst. *Chinese J. Cataly*., **2008**, *29*, 105.

[67] Gombac, V.; Sordelli, L.; Montini, T.; Delgado, J. J.; Adamski, A.; Adami, G.; Cargnello, M.; Bernal, S.; Fornasiero, P. CuO_x-TiO_2 photocatalysts for H_2 production from ethanol and glycerol solutions. *J. Phys. Chem. A*, **2010**, *114*, 3916 –3925

[68] Huang L.; Peng, F.; Yu, H.; Wang, H. Preparation of cuprous oxides with different sizes and their behaviors of adsorption, visible-light driven photocatalysis and photocorrosion. *Solid State Sciences*, **2009**, *11*, 129-138.

[69] Barreca, D.; Fornasiero, P.; Gasparotto, A.; Gombac, V.; Maccato, C.; Montini, T.; Tondello, E.; The Potential of Supported Cu_2O and CuO Nanosystems in Photocatalytic H_2 Production. *ChemSusChem*, **2009**, *2*, 230-233.

[70] Maccato, C.; Barreca, D.; Carraro, G.; Gasparotto, A.; Gombac, V.; Fornasiero, P. Photoassisted H_2 production by metal oxide nanomaterials fabricated through CVD-based approaches. *Surface & Coatings Technology*, **2013**, *230*, 219-227.

[71] Carraro, G.; Gasparotto, A.; Maccato, C.; Gombac, V.; Rossi, F.; Montini, T.; Peeters, D.; Bontempi, E.; Sada, C.; Barreca, D.; Fornasiero, P. Solar H_2 generation via ethanol photoreforming on Fe_2O_3 nanorod arrays activated by Ag and Au nanoparticles. *RSC Advances*, **2014**, *4*, 32174-32179.

TOC

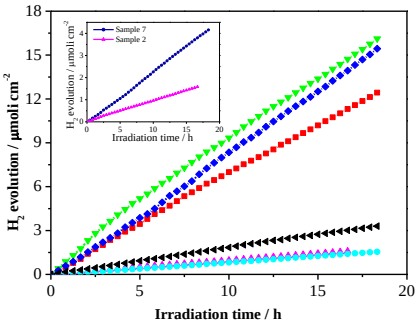
H2 evolution / μmoli cm-2
Irradiation time / h
Sample 7
Sample 2
H2 evolution / μmoli cm-2
Irradiation time / h